



Article

Layout Optimization and Performance Analysis of Vehicle Suspension System Using an Electromagnetic Inerter

Chen Luo , Xiaofeng Yang * , Zhihong Jia and Changning Liu

School of Automotive and Traffic Engineering, Jiangsu University, Zhenjiang 212013, China; 2222104151@stmail.ujs.edu.cn (C.L.); 2212304004@stmail.ujs.edu.cn (Z.J.); cn271828@163.com (C.L.)

* Correspondence: yangxf18@ujs.edu.cn

Abstract: The inerter is a vibration isolation device used to replace the mass element in classical vibration isolation theory. The introduction of an inerter into a vehicle suspension system can greatly improve the performance of the system. An electromagnetic inerter is a kind of device that can realize a complex suspension structure without an additional energy supply and a complicated control system. It not only utilizes hydraulic systems to attain various suspension mechanical structures but also incorporates linear generators to form more intricate electrical networks. In this paper, an approach is proposed to achieve an optimized vehicle suspension layout using an electromagnetic inerter, which promotes the practical application of the device. First, seven suspension layouts are presented based on this device and relevant models are established to optimize the performance of these seven layouts under certain objectives. Then, the influence of three factors of the electrical network, namely linear generator internal resistance, inductance, and linear generator coefficient, on suspension performance is analyzed. At the same time, to ensure the suspension performance of this device is closer to that required for actual engineering applications, the improvement in the vibration isolation performance of the device compared with traditional passive suspension is discussed considering these three factors. The final results show that when considering the real-world situation, the L1 and L4 layouts can achieve excellent performance improvement, with RMS(BA) values of only 85.73% and 84.66% of the traditional passive suspension.

Keywords: vehicle suspension system; electromagnetic inerter; layout optimization; performance analysis



Citation: Luo, C.; Yang, X.; Jia, Z.; Liu, C. Layout Optimization and Performance Analysis of Vehicle Suspension System Using an Electromagnetic Inerter. *World Electr. Veh. J.* **2023**, *14*, 318. <https://doi.org/10.3390/wevj14120318>

Academic Editor: Joeri Van Mierlo

Received: 18 October 2023

Revised: 8 November 2023

Accepted: 11 November 2023

Published: 22 November 2023



Copyright: © 2023 by the authors. Licensee MDPI, Basel, Switzerland. This article is an open access article distributed under the terms and conditions of the Creative Commons Attribution (CC BY) license (<https://creativecommons.org/licenses/by/4.0/>).

1. Introduction

As a key system in the vehicle chassis, the performance of the suspension system determines whether a vehicle can safely drive on the road while ensuring the comfort of passengers and the integrity of freight. Many scholars have proposed various new structures and design methods for suspension systems, aiming to increase the system dynamics performance of vehicles to a higher level. Examples include a semi-active suspension that could change the damping coefficient of the damper [1–4], a pneumatic suspension with adjustable ride height and spring stiffness [5], a quasi-zero-stiffness suspension system with characteristics of high static load and low dynamic load [6,7], and an active suspension that introduces a force generator [8,9]. These solutions have been shown to significantly improve suspension performance, but often require an additional energy supply or a larger suspension structure to achieve the relevant functions.

The “mass–spring–damper” configuration in classical vibration isolation theory is widely used in the field of mechanical vibration isolation [10–13]; however, due to the volume and weight of the mass element, its application is greatly limited. Since the inerter was invented by Prof. Smith in 2002 [14], the traditional vibration isolation theory has been improved and has appeared in the form of “inerter–spring–damper”. The implementation of this has been attempted in bridges [15,16], floating offshore wind turbines [17,18], aircrafts [19], etc. The excellent vibration suppression ability of the vibration isolation

system, based on the new vibration isolation theory, has been proven. Since the inerter is a two-end element, it can achieve a large virtual mass at the cost of a relatively small volume and weight. For example, the fluid inerter described in [20] can achieve an inertance coefficient of up to 219 kg with a fluid mass of only 0.4 kg. Thus, its combination with vehicle suspension is a potential solution to improve the performance of the suspension system [21].

At present, there have been many cases of trying to introduce the inerter into a vehicle suspension system. Shen et al. replaced the mass element in the dynamic vibration absorber with an inerter and applied it to a suspension system, achieving frequency-domain characteristics similar to those obtained when adding a dynamic shock absorber to the body mass [22]. Hu et al. tried to combine skyhook control with an inerter and proposed three different control laws, improving the control effect by more than 10% compared with the traditional structure, and finally proving that the ride comfort of the vehicle was greatly improved [23]. Liu et al. studied the road-friendly performance of heavy vehicles under three different layouts, and the results showed that using an inerter in the suspension system of heavy vehicles can significantly reduce road damage [24].

Researchers found that numerous suspension layouts can be achieved based on the combination of the spring, damper, and inerter, and many of them have excellent dynamic performance. Thus, methods to implement these complex suspension structures have become a research hotspot. One method is to use the existing mechanical structure to achieve the structure design. For example, Liu et al. explored a scheme for implementing complex layouts with a fluid inerter [20,25]. Another approach is to introduce the concept of mechanical–electrical analogy [26] into the design process and use electrical elements instead of mechanical elements in vibration isolation systems. This method requires a “speed-to-voltage” conversion mechanism, which is usually a generator. Wang and Chan combined a ball screw inerter and permanent magnet electric machinery (PMEM) to realize the comprehensive design of a mechanical network and an electrical network, which greatly reduced the difficulty of an integrated design of a complex vibration isolation system [27]. A hydraulic electric inerter (HEI) device composed of a linear generator and hydraulic piston was proposed by Shen et al. [28]. This device eliminates the influence of nonlinear factors, such as back clearance, friction, and elastic deformation, by omitting the parts that convert between rotating motion and displacement motion.

The relevant research in this paper will be based on an electromagnetic inerter (EMI), a new vibration isolation device [29]. This device consists of a linear generator and a piston cylinder with a helical tube around the cylinder extensine. The external port of the linear generator can be connected to an external circuit to form an electrical network; this capability enables the establishment of a vibration isolation network with a complex layout. The helical tube is connected to the upper and lower chambers of the piston cylinder, forming the same structure as the fluid type inerter described in [23]. In addition to the use of electronic elements to simulate complex structures, this electromechanical coupling-type inerter can also realize the series of damping element and inertance element in the mechanical network [20], which is impossible for the two electromechanical coupling-type inerters mentioned above. The Electromagnetic Inerter–Spring–Damper (EM-ISD) Suspension System is the vehicle suspension system which uses the EMI as the main vibration suppression component. Since it is essentially a passive suspension system, it does not require sensors, controllers, and other equipment required for semi-active or active suspension, or energy input.

The rest of this paper is organized as follows: In Section 2, seven feasible suspension layouts are listed, along with the optimization methods and objectives used to obtain the optimal suspension parameters. In Section 3, the performance characteristics of the seven suspension layouts mentioned above are obtained under ideal conditions. In Section 4, the effects of internal resistance and internal inductance of a linear generator are discussed, and attempts are made to incorporate them into the optimization process in order to obtain optimization results that are more aligned with engineering practice. In Section 5, the

influence of the nonlinear parameter K_m , a coefficient of the linear generator, on suspension performance is shown. In Section 6, the dynamic characteristics of suspension systems using EMI are demonstrated, while the differences between suspension systems and traditional passive suspension systems in the frequency domain are analyzed. Finally, some conclusions are presented in Section 7.

2. Layout Optimization Method of EM-ISD Suspension System

The vehicle quarter suspension model with EM-ISD suspension is shown in Figure 1. The red dashed box shows the suspension layout that EMI can achieve, encompassing both the mechanical components and the equivalent structure simulated by the external circuit. In the blue dot box on the right, there is a list of eight three-element layouts that will be implemented by electronic components in the form of external circuits. Their equivalent relationship follows the second type of mechanical–electrical analogy theory, namely resistance equivalent damping, capacitance equivalent inerter, and inductance equivalent spring. Due to the repetitive components in layout L2 and layout L6, the spring element of the equivalent structure in layout L2 and the entire layout L6 should be discarded. Finally, the layouts L1, L3, L4, L5, L7, L8, and the modified L2 were investigated.

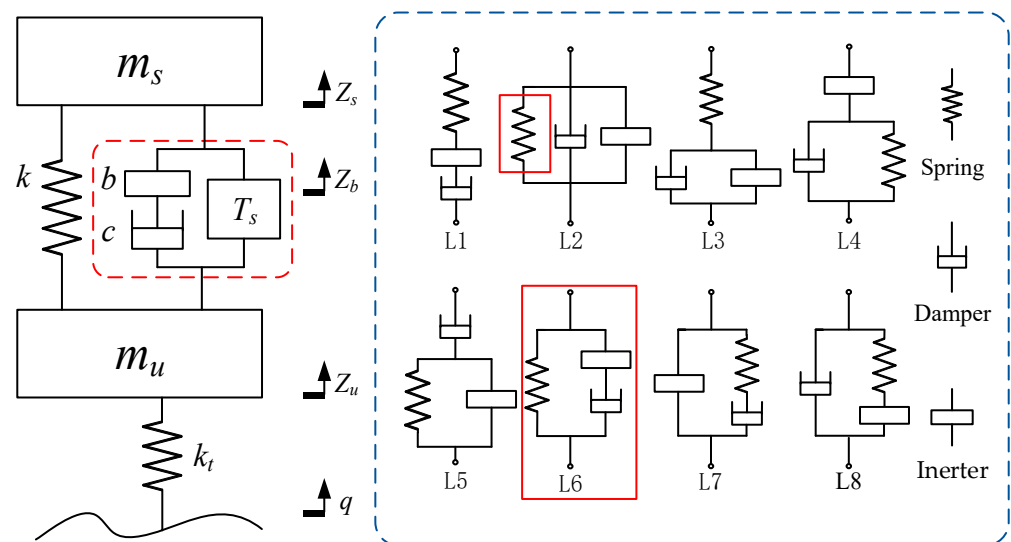


Figure 1. The quarter suspension model and eight layouts.

The dynamic equations are presented in Equation (1), where m_s and m_u represent the sprung mass and unsprung mass, respectively. z_s , z_u , and z_b represent the displacement of the sprung mass, unsprung mass, and one terminal of the inerter element. k and k_t are the main spring stiffness and tire equivalent stiffness. q is the uneven road displacement. T_s represents the equivalent external circuit, typically expressed as a velocity-type impedance expression.

$$\begin{cases} m_s \ddot{z}_s + k(z_s - z_u) + T_s(\dot{z}_s - \dot{z}_u) + u = 0 \\ m_u \ddot{z}_u + k_t(z_u - q) - k(z_s - z_u) - T_s(\dot{z}_s - \dot{z}_u) - u = 0 \\ u = b(\ddot{z}_u - \ddot{z}_b) = c(\dot{z}_b - \dot{z}_u) \end{cases} \quad (1)$$

To obtain the appropriate parameters of the EM-ISD suspension system, the design process incorporates the particle swarm optimization (PSO) method. This is a swarm intelligence optimization algorithm that was developed in 1995 [30,31]. It considers not only the collective behavior of simulated organisms but also individual cognition and social influence. The logic of this algorithm is simple enough to be implemented in just a few lines of code, and it can be easily modified to accommodate multi-threaded computing

devices, thereby significantly increasing the speed of optimization. The flow chart is shown in Figure 2.

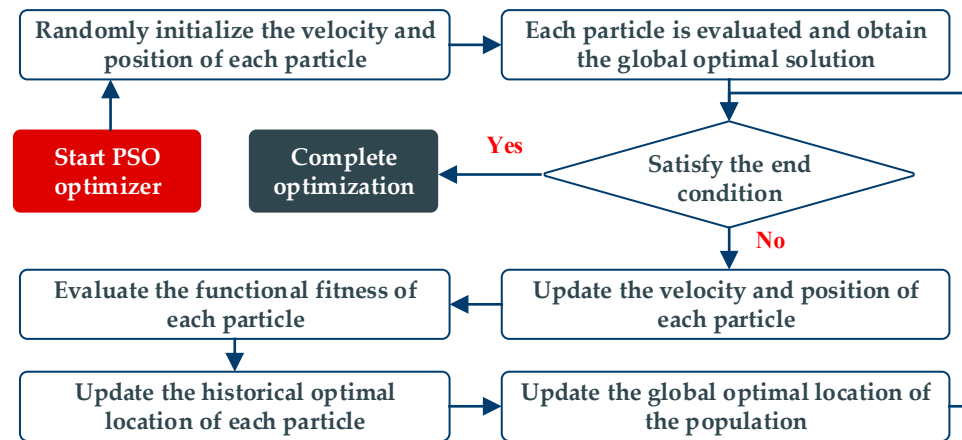


Figure 2. The flow chart and pseudocode of PSO.

For convenience, the root mean square (RMS) values of body acceleration (BA), suspension working space (SWS), and dynamic tire load (DTL) are simply denoted as RMS(BA), RMS(SWS), and RMS(DTL). These three performance indicators express the ability of the vehicle suspension system to isolate vibrations. By setting the optimization objective as Equation (2), the $RMS(BA_{EM-ISD})$ can be minimized while ensuring that $RMS(SWS_{EM-ISD})$ and $RMS(DTL_{EM-ISD})$ are not weaker than the traditional passive suspension.

$$\begin{cases} \text{Obj} = \text{RMS}(BA_{EM-ISD}); \\ \text{RMS}(DTL_{EM-ISD}) < \text{RMS}(DTL_{PA}); \\ \text{RMS}(SWS_{EM-ISD}) < \text{RMS}(SWS_{PA}). \end{cases} \quad (2)$$

The optimization process described above considers the road condition as a randomly excited pavement, with the surface profile represented by Equation (3).

$$\dot{q}(t) = -2\pi f_0 q(t) + 2\pi \sqrt{G_0} v \omega(t) \quad (3)$$

where $q(t)$ represents the road input, $\omega(t)$ represents the white noise with zero mean, f_0 denotes the lower cutoff frequency, v represents the vehicle speed, and G_0 represents the road roughness coefficient. Concrete values are presented in Table 1.

Table 1. The basic parameters of the road model.

Parameter [Unit]	Value
Lower cut-off frequency f_0 [Hz]	0.01
Vehicle speed v [m/s]	20
Road roughness coefficient G_0 [m^3/cycle]	256×10^{-6}

Table 2 lists all the parameters of the traditional passive suspension that will be used for comparison. The subsequent optimization will be implemented using the performance of this suspension as the benchmark indicator.

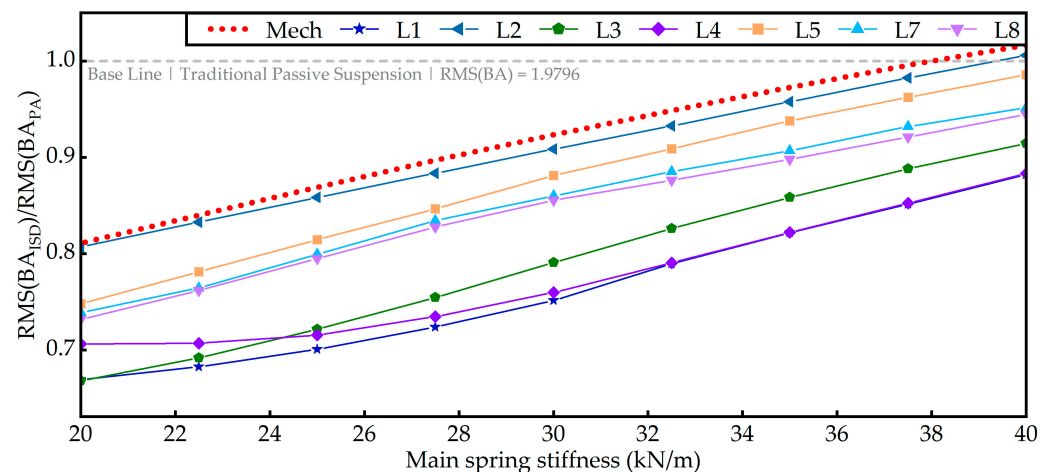
In order to optimize these suspension layouts, the sprung mass, unsprung mass, and tire equivalent stiffness should be consistent with those of the traditional passive suspension, as shown in Table 2. The value of suspension spring stiffness ranges from 20 kN/m to 40 kN/m, with an increment of 2.5 kN/m. The remaining suspension parameters that need to be optimized include the inertance coefficient and damping coefficient in the mechanical network, as well as the inertance coefficient, damping coefficient, and spring stiffness simulated by the electrical network.

Table 2. Traditional passive suspension base parameters for comparison.

Parameter [Unit]	Value
Suspension spring stiffness k [N/m]	35,000
Tire equivalent stiffness k_t [N/m]	190,000
Sprung mass m_s [kg]	400
Unsprung mass m_u [kg]	45
Damping coefficient c [N/(m/s)]	1850

3. Performance of EM-ISD Suspension under Ideal Conditions with Different Main Spring Stiffness

Figure 3 shows the optimization results, with the main spring stiffness on the horizontal axis and the RMS(BA) ratio of the EM-ISD suspension to the traditional passive suspension on the vertical axis. The dashed gray line represents the optimization baseline. Performance below this line can be considered superior to the traditional passive suspension mentioned above. The RMS(BA) is represented by the red dot line when the external circuit is not included in the EM-ISD suspension. As can be seen from Figure 3, when the suspension main spring stiffness is 35 kN/m, the EM-ISD suspension exhibits clear advantages over the traditional passive suspension. The RMS(BA) values of the L1 and L4 layouts are only 82.19% and 82.22%, respectively, compared to the traditional passive suspension. When the stiffness of the main suspension spring is less than 32.5 kN/m, there will be a significant difference in the performance of L1 and L4, with L1 exhibiting a better vibration isolation performance. Although the RMS(BA) of the L3 layout appears to be better than both the L1 and L4 layouts when the main spring stiffness is reduced to 20 kN/m. However, the main spring also serves the function of supporting the weight of the body. When the stiffness value of the main spring is too low, a large compression of the spring is required to support the entire body, which will greatly restrict the working space of the suspension. Therefore, blindly pursuing a low mainspring stiffness does not make sense in engineering applications.

**Figure 3.** The optimization results of the main objective.

At the same time, the advantages brought about by the introduction of electrical networks are also significant. The curves of seven structures, ranging from L1 to L8 layouts, are all below the red dot line. Therefore, it can be considered that regardless of which external circuit connected, there will be varying degrees of improvement in performance amplitude compared to the pure mechanical structure of the EM-ISD suspension.

Moreover, the EM-ISD suspension, which achieves a complex suspension structure through the external circuit, also has a greater ability to coordinate the three performance indicators of RMS(BA), RMS(SWS), and RMS(TDL). As depicted in Figure 4, particularly the

L1 and L4 layouts mentioned previously, they appear to be more favorable for minimizing the demands on RMS(TDL) and RMS(SWS) in order to attain a lower RMS(BA).

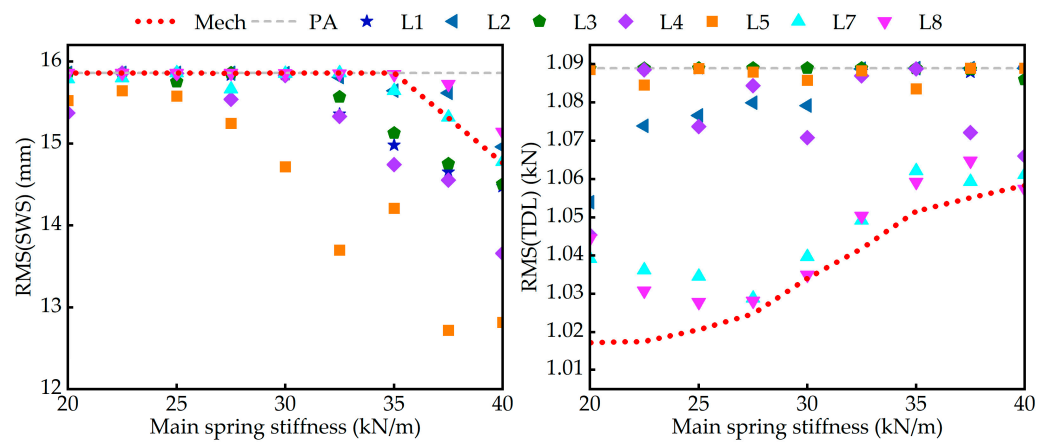


Figure 4. The performance of optimized suspension in terms of RMS(SWS) and RMS(TDL).

4. EMI-ISD Suspension Considering Internal Resistance and Inductance of Linear Generator

In the above optimization process, the internal resistance (R_a) and inductance (L_a) of the linear generator are ignored, even though they are typically recognized to have an impact on the suspension performance [32]. In an electrical network, R_a and L_a can be considered to be in a series with the external network. The L1 layout demonstrates excellent performance within the main spring stiffness range of 20 kN/m to 40 kN/m. Therefore, the upcoming research will be conducted using this layout. The values of R_a and L_a are restricted to a range of 0-1 Ω and 0-50 mH, respectively. Equation (4) illustrates the numerical conversion relationship between mechanical and electronic components. Where K_m is the coefficient of the linear generator; C , R , and L represent the numerical values of capacitance, resistance, and inductance, respectively; and b , c , and k represent the coefficients of inertance, damping, and spring stiffness, respectively [28]. When K_m is 8100, the equivalent damping and equivalent stiffness of R_a and L_a range from 8100 N/(m/s) to infinity and 162,000 N/m to infinity, respectively.

$$C = \frac{b}{K_m}, R = \frac{K_m}{c}, L = \frac{K_m}{k} \tag{4}$$

In Figure 5, the performance of the EM-ISD suspension significantly deteriorates across the board with the increase in R_a . When the R_a is increased, RMS(BA) still offers significant advantages over mechanical ISD suspensions and traditional passive suspensions. But RMS(SWS) and RMS(TDL) are significantly worse than the traditional passive suspension.

Compared with R_a , L_a has a relatively small impact on EM-ISD suspension and the decreasing trend of RMS(SWS) with the increase of L_a in Figure 6 is even more surprising. However, deterioration still occurs in the RMS(TDL).

The above results show that R_a and L_a are two factors that must be taken into account in the design. R_a and L_a should be considered as two inherent parameters in the electrical network. The modified electrical network is shown in Figure 7, where L_a is 26 mH and R_a is 0.38 Ω . The “G” stands for the linear generator, which performs the function of converting velocity into voltage.

In Figure 8, three sets of RMS(BA) values are shown. The L1 and L4 layouts shown in Figure 3 can achieve better vibration isolation performance compared to the other five layouts under ideal conditions. However, once the effects of R_a and L_a are considered in the study, the dynamic characteristics of these suspension layouts will change significantly, particularly the L1 layout. If the negative effects of R_a and L_a are addressed by incorporating them into the optimization process, the impact of R_a and L_a on RMS(BA) is less than 0.5% in both layouts.

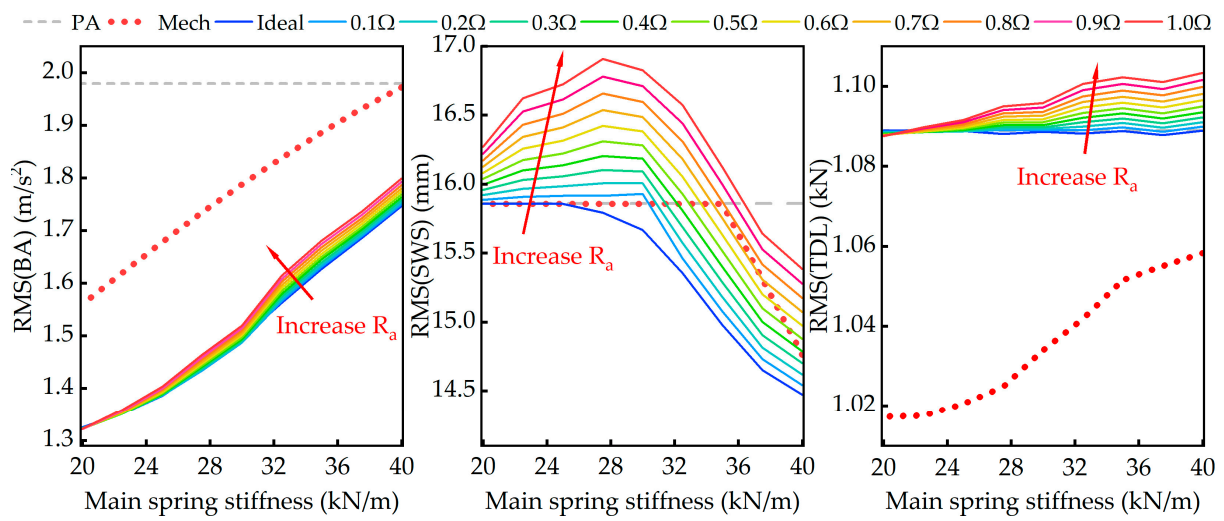


Figure 5. Performance change in EMI-ISD suspension with R_a increase.

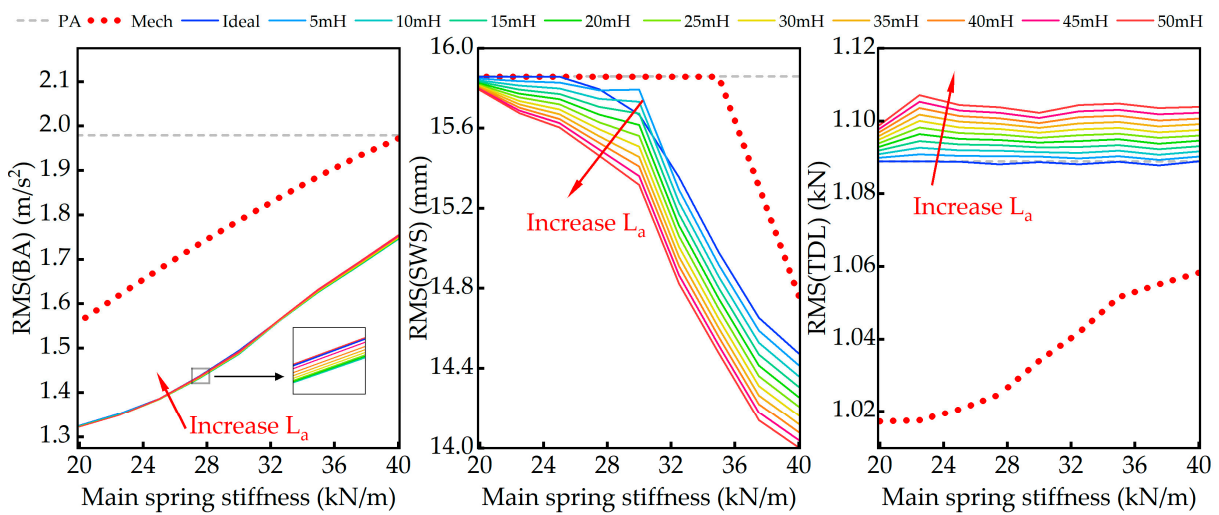


Figure 6. Performance change in EMI-ISD suspension with L_a increase.

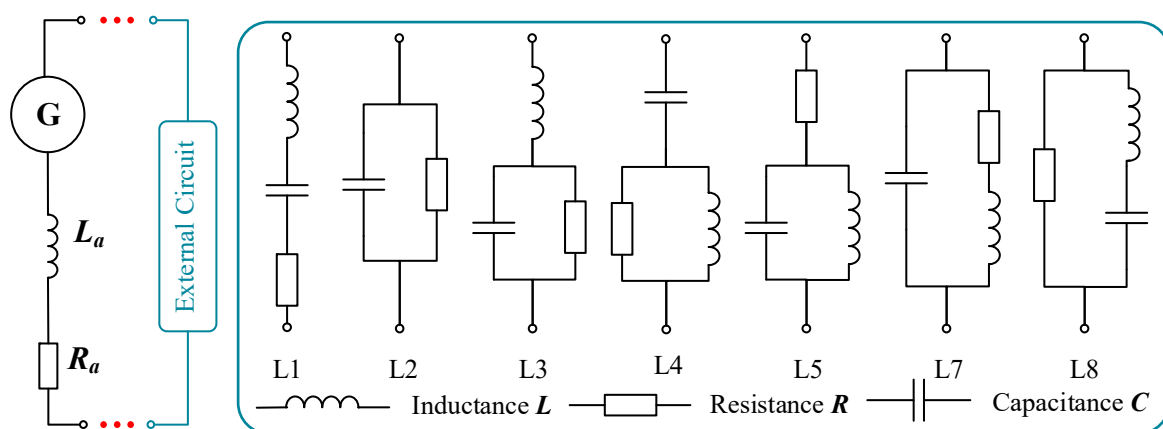


Figure 7. Modified electrical network.

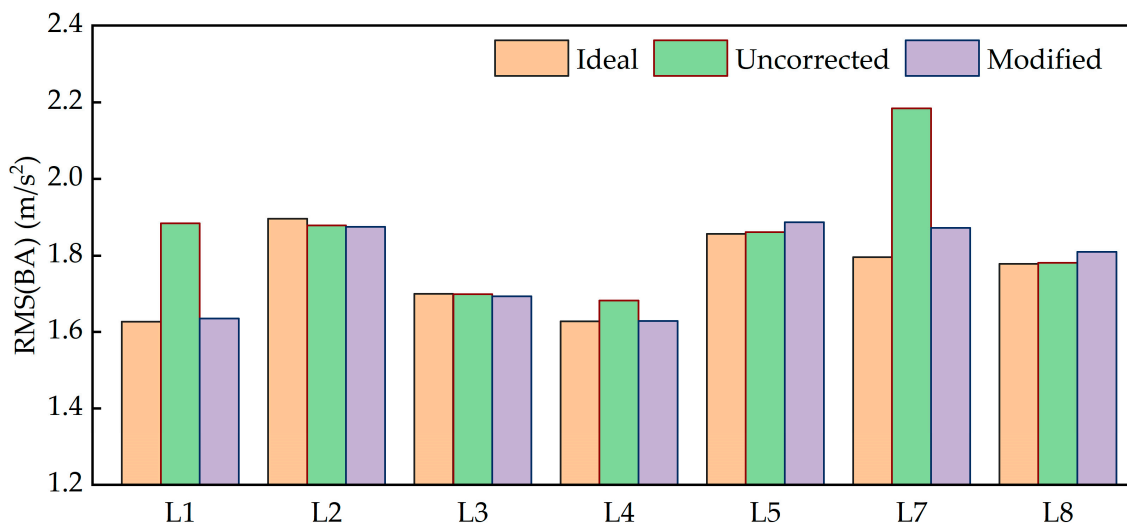


Figure 8. The results of RMS(BA) under ideal conditions, uncorrected conditions, and corrected conditions, respectively.

A particularly interesting phenomenon occurs in the L2 layout. When the influence of R_a and L_a is introduced, the RMS(BA) of L2 is lower than that of the ideal condition, regardless of whether the parameter is modified or not. This may be due to the presence of R_a and L_a , which increase the order of the transfer function of the vibration isolation system. As shown in Equations (5) and (6), the highest order of L2 layout in an ideal state is only a quadratic term. However, due to the presence of R_a and L_a , the highest order is raised to three. The order of the suspension transfer function affects the performance of the suspension system. Generally, the higher the order, the greater the vibration isolation ability.

$$T_{L2}(s) = \frac{1}{\frac{1}{bs} + \frac{1}{c}} + c_e + b_e s = \frac{bb_e s^2 + (bc + bc_e + b_e c)s + cc_e}{bs + c} \tag{5}$$

$$T_{L2_Modified}(s) = \frac{1}{\frac{1}{bs} + \frac{1}{c}} + \frac{1}{\frac{1}{c_e + b_e s} + \frac{1}{R_a} + \frac{L_a}{s}} \tag{6}$$

$$= \frac{(R_a c + R_a b b_e c) s^2 + (R_a b + bc + R_a b c c_e) s + L_a R_a b c}{R_a b_e c s^3 + (c(R_a c_e + 1) + R_a b b_e) s^2 + (b(R_a c_e + 1) + L_a R_a c) s + L_a R_a b}$$

5. Nonlinear Factor of Linear Generator Coefficient

K_m has often been assumed to be a constant value in previous studies, which is reasonable in most cases. However, electromagnetic systems typically exhibit strong nonlinear characteristics. Additionally, the limitations of vehicle suspension installation space and the inherent properties of ferromagnetic materials amplify the effects on K_m . Therefore, the assumption of simple linearization cannot be well established in practical applications. As shown in Figure 9, when a 10 Ω resistor is connected in series at the external port, the results obtained by the Finite Element Method (FEM) differ significantly from the predictions of the ideal simplified model as the relative velocity between the stator and the actuator increases to 0.3 m/s. When the velocity increases, the output force of the linear generator initially shows an increasing trend. However, this trend gradually diminishes, resulting in a significant decrease in the value of K_m as the velocity increases. K_m can be calculated using Equation (7), where R represents the resistance value of the external circuit connection, F represents the magnitude of the electromagnetic force, and V represents the relative motion velocity of the linear generator [28].

$$K_m = RF/V \tag{7}$$

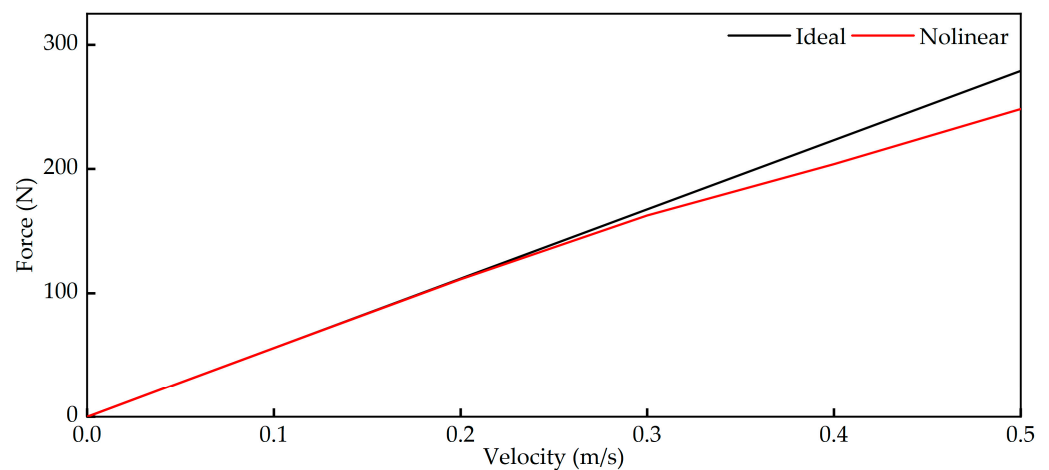


Figure 9. Linear generator force–velocity curve (external 10 Ω resistor).

To observe the effect of this nonlinear condition on performance, K_m is set to a value that can vary with velocity. Key values are obtained by referring to the nonlinear curve in Figure 9, as indicated in Table 3. The K_m values for other speeds will be obtained by fitting.

Table 3. The relationship between K_m and velocity.

Velocity [m/s]	0	0.1	0.2	0.3	0.4	0.5
K_m	558.3473	558.3473	553.8494	515.3094	411.0438	444.4875

As shown in Figure 10, the RMS(BA) of the seven layouts exhibit significant changes when K_m is related to the relative motion velocity of the suspension compared to the ideal EM-ISD suspension. As shown in Table 4, the RMS(BA) of all seven layouts is still lower than that of the traditional passive suspension under this condition. In particular, for the two layouts, L1 and L4, their RMS(BA) is only 85.73% and 84.66% compared to the traditional passive suspension.

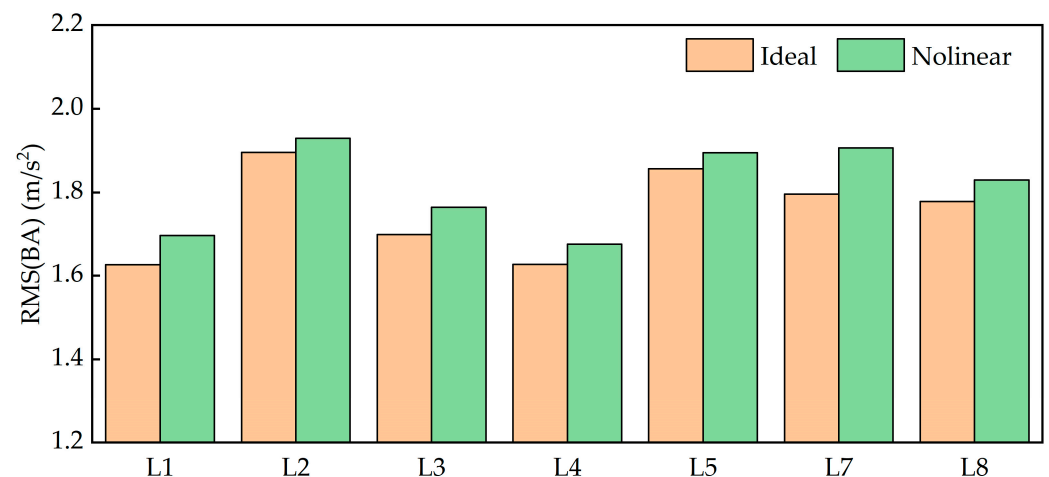


Figure 10. Optimization results with and without considering the nonlinear characteristics of K_m .

Table 4. Comparison of performance losses.

	L1	L2	L3	L4	L5	L7	L8
$\text{RMS}(\text{BA}_{\text{ISD_Ideal}})/\text{RMS}(\text{BA}_{\text{PA}})$	82.20%	95.76%	85.85%	82.22%	93.79%	90.71%	89.82%
$\text{RMS}(\text{BA}_{\text{ISD_Nolinear}})/\text{RMS}(\text{BA}_{\text{PA}})$	85.73%	97.44%	89.15%	84.66%	95.72%	96.30%	92.41%

6. Dynamic Characteristics of EM-ISD under Random Pavement

The results of Sections 4 and 5 reveal that the L1 and L4 layouts still have a high potential for vibration isolation after modification. In this section, the performance characteristics of the EM-ISD suspension system are discussed, taking into account factors such as internal resistance, inductance, and the unsteady coefficient K_m of the linear generator. The frequency and time domain characteristics of the EM-ISD suspension under random road excitation are displayed.

Figures 11 and 12 depict the characteristics of vehicle acceleration under L1 and L4 layouts, respectively, in the form of time-domain and power spectral density (PSD) plots. Compared to traditional passive suspension, the inclusion of EMI significantly decreases the PSD of body acceleration at 1–2 Hz. At the same time, due to the influence of nonlinear factors, the PSD of L1 and L4 layouts is slightly higher than the value under ideal conditions at frequencies above 5 Hz. It is worth noting that the influence of nonlinear factors reduces the PSD of the body acceleration in the 1–2 Hz band.

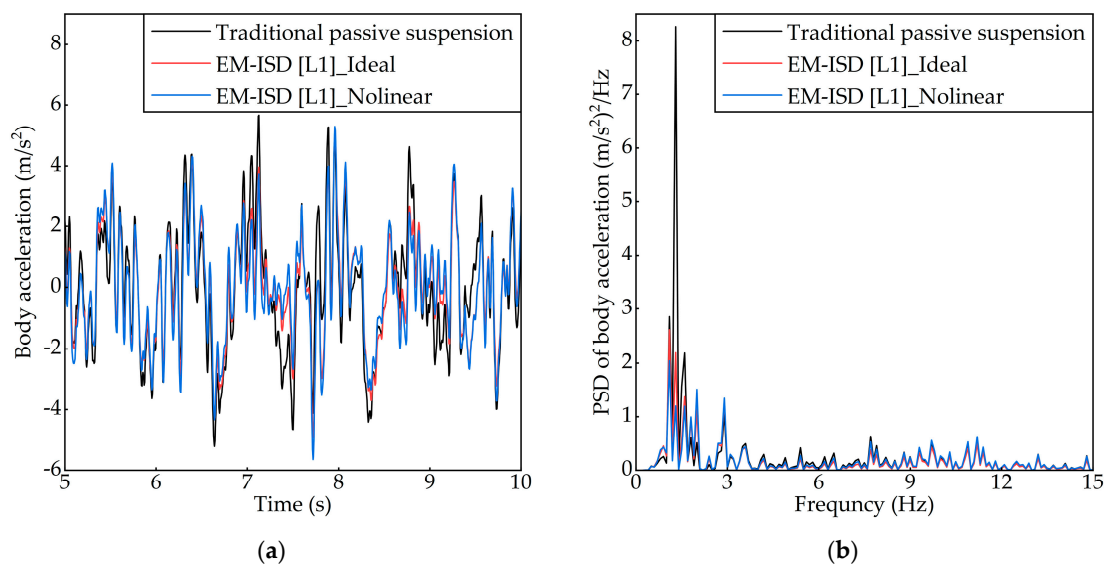


Figure 11. Dynamic performance of EM-ISD [L1] suspension layout in terms of body acceleration. (a) Body acceleration in the time domain; (b) PSD of body acceleration.

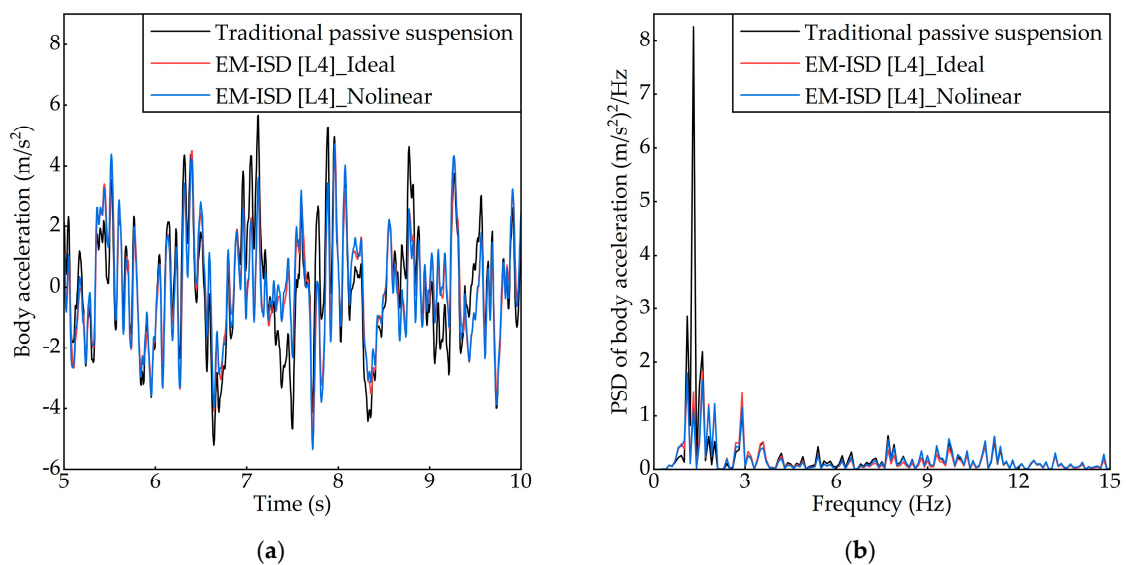


Figure 12. Dynamic performance of EM-ISD [L4] suspension layout in terms of body acceleration. (a) Body acceleration in the time domain; (b) PSD of body acceleration.

The RMS(DTL) and RMS(SWS) of the EMI-ISD suspension are essentially identical to those of the traditional passive suspension. However, there are notable distinctions in PSD. As shown in Figure 13, the tire dynamic load PSD of the EM-ISD suspension exhibits a notable decrease at frequencies between 1 and 2 Hz, while showing a slight increase at frequencies above 5 Hz, in comparison to the traditional passive suspension. As shown in Figure 14, the peak PSD of the suspension working space is shifted after the application of EMI, and its frequency is lower compared to that of the traditional passive suspension. More importantly, the maximum peak value is also reduced compared to the traditional suspension.

The optimized parameters to achieve the above EM-ISD suspension performance are shown in Table 5. R , C , and L respectively represent the resistance, capacitance, and inductance in the external circuit, forming an electrical network to simulate a complex mechanical structure. The inertance coefficient and damping coefficient in the mechanical network are represented as b and c .

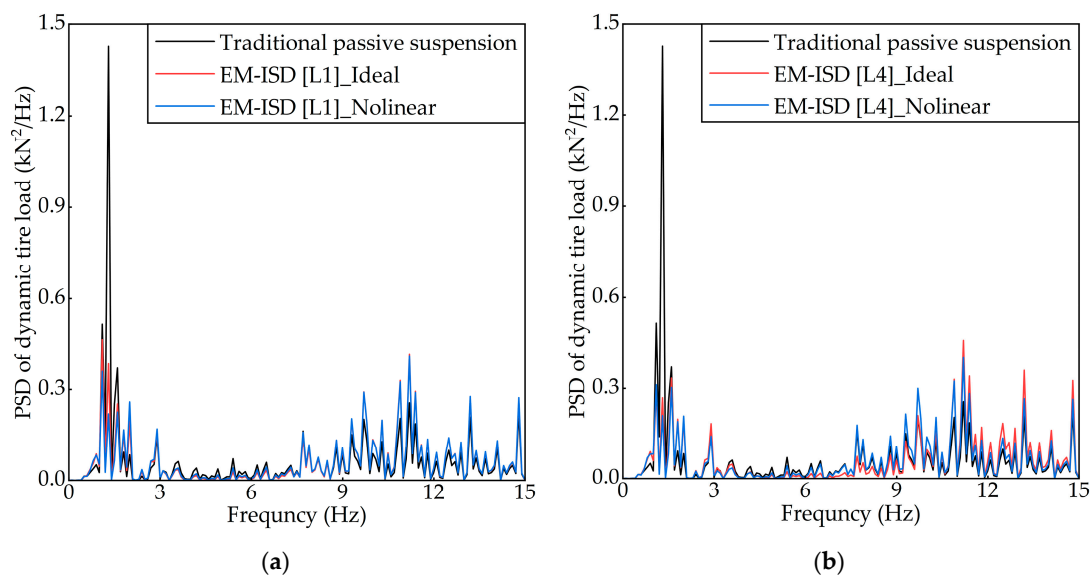


Figure 13. The PSD of dynamic tire load. (a) EM-ISD [L1] layout; (b) EM-ISD [L4] layout.

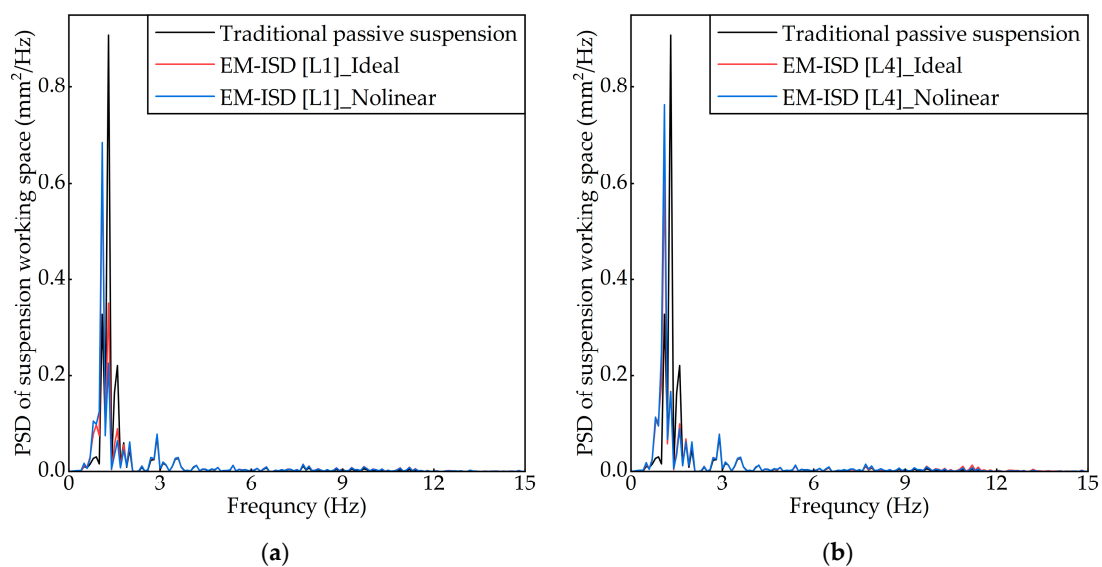


Figure 14. The PSD of suspension working space. (a) EM-ISD [L1] layout; (b) EM-ISD [L4] layout.

Table 5. Optimal parameters of EM-ISD suspension system.

	R [Ω]	C [mF]	L [mH]	b [kg]	C [N/(m/s)]
EM-ISD [L1]_Nolinear	0.84	46.73	197.82	85.23	1617.11
EM-ISD [L4]_Nolinear	6.48	44.09	256.73	36.54	1199.36

7. Conclusions

This paper attempts to apply EMI to vehicle suspension. Firstly, the corresponding quarter-suspension model is established, and the suspension layouts are realized using external electrical components. Then, the optimal parameters of the suspension structure are obtained using the PSO optimization algorithm. The simulation results show that the EM-ISD suspension has significant advantages over the traditional passive suspension, particularly for layouts L1 and L4. On this basis, three factors that need to be addressed in the practical application process are considered: internal resistance R_a , internal inductance L_a , and the linear generator coefficient K_m . The results show that if these factors are ignored during the simulation stage, the engineering practice of the EM-ISD suspension will exhibit dynamic characteristics that are completely different from the simulation. However, if these factors are considered in the optimization process, more realistic simulation results can be obtained. This will provide a more comprehensive theoretical basis for the development of the EM-ISD suspension. Finally, the performance characteristics of EM-ISD [L1] suspension and EM-ISD [L4] suspension in both the frequency domain and time domain are demonstrated. The results show that the EM-ISD suspension differs significantly from traditional passive suspension in the frequency domain. This finding demonstrates that the EM-ISD suspension is highly effective in suppressing body vibrations at the offset frequency. The RMS(BA) of EM-ISD [L1] and EM-ISD [L4] can be reduced to 85.73% and 84.66% of traditional passive suspensions, respectively, after considering three factors that are present in practical applications.

Viscous resistance must exist when a fluid flows through a helical tube, and this resistance is determined by the inherent properties of the fluid. The viscous resistance in the helical tube can be considered as a damper that directly connects the sprung and unsprung masses. This paper does not discuss the effect of viscous resistance, mentioned above, on the output characteristics of EMI when the damping component and the inertance component of the fluid structure are connected in series. In future research, it is important to carefully consider the influence of this factor on the performance of the EM-ISD suspension. Additionally, experimental research will be conducted to further evaluate the performance of the EM-ISD suspension system.

Author Contributions: Conceptualization, C.L. (Chen Luo) and X.Y.; methodology, C.L. (Chen Luo); software, C.L. (Chen Luo); validation, X.Y., Z.J. and C.L. (Changning Liu); formal analysis, C.L. (Chen Luo), X.Y. and Z.J.; investigation, C.L. (Chen Luo); resources, X.Y. and C.L. (Changning Liu); data curation, C.L. (Chen Luo) and Z.J.; writing—original draft preparation, C.L. (Chen Luo); writing—review and editing, Z.J.; visualization, C.L. (Chen Luo) and Z.J.; supervision, X.Y. and C.L. (Changning Liu); project administration, X.Y. and C.L. (Changning Liu); funding acquisition, C.L. (Chen Luo), X.Y. and C.L. (Changning Liu). All authors have read and agreed to the published version of the manuscript.

Funding: This work was supported by the National Natural Science Foundation of China [Grant No. 52072157, 52202471]; Jiangsu Funding Program for Excellent Postdoctoral Talent [Grant No. 2022ZB659]; Postgraduate Research & Practice Innovation Program of Jiangsu Province [Grant number: SJCX22_1852].

Data Availability Statement: Data are contained within the article.

Conflicts of Interest: The authors declare no conflict of interest.

References

1. Savaresi, S.M.; Silani, E.; Bittanti, S. Acceleration-Driven-Damper (ADD): An Optimal Control Algorithm For Comfort-Oriented Semiactive Suspensions. *J. Dyn. Syst. Meas. Control* **2005**, *127*, 218–229. [[CrossRef](#)]
2. Morselli, R.; Zanasi, R. Control of Port Hamiltonian Systems by Dissipative Devices and its Application to Improve the Semi-Active Suspension Behaviour. *IFAC Proc. Vol.* **2006**, *39*, 548–553. [[CrossRef](#)]
3. Karnopp, D.; Crosby, M.J.; Harwood, R.A. Vibration Control Using Semi-Active Force Generators. *J. Eng. Ind.* **1974**, *96*, 619–626. [[CrossRef](#)]
4. Aljarbouh, A.; Fayaz, M. Hybrid Modelling and Sliding Mode Control of Semi-Active Suspension Systems for Both Ride Comfort and Road-Holding. *Symmetry* **2020**, *12*, 1286. [[CrossRef](#)]
5. Yin, Z.; Khajepour, A.; Cao, D.; Ebrahimi, B.; Guo, K. A New Pneumatic Suspension System with Independent Stiffness and Ride Height Tuning Capabilities. *Veh. Syst. Dyn.* **2012**, *50*, 1735–1746. [[CrossRef](#)]
6. Chen, L.; Wang, J.; Xu, X.; Jiang, X.; Wang, F. Nonlinear Analysis of a Quasi-Zero Stiffness Air Suspension Based on the Cell-Mapping Method. *Int. J. Acoust. Vib.* **2021**, *26*, 148–160. [[CrossRef](#)]
7. Abolfathi, A. Can a Nonlinear Quasi-Zero-Stiffness Spring Improve the Ride Quality of a Vehicle? *Veh. Syst. Dyn.* **2023**, 1–17. [[CrossRef](#)]
8. Sun, W.; Zhao, Z.; Gao, H. Saturated Adaptive Robust Control for Active Suspension Systems. *IEEE Trans. Ind. Electron.* **2013**, *60*, 3889–3896. [[CrossRef](#)]
9. Li, H.; Yu, J.; Hilton, C.; Liu, H. Adaptive Sliding-Mode Control for Nonlinear Active Suspension Vehicle Systems Using T-S Fuzzy Approach. *IEEE Trans. Ind. Electron.* **2013**, *60*, 3328–3338. [[CrossRef](#)]
10. Jin, C.; Dong, Y.; Guan, X.; Zhou, J.; Wang, F. Design and Vibration Suppression Performance of Magnetic Suspension Dynamic Vibration Absorber. *J. Vib. Control* **2021**, *27*, 2420–2431. [[CrossRef](#)]
11. Xu, Q.; Niu, J.; Yao, H.; Zhao, L.; Wen, B. Nonlinear Dynamic Behavior and Stability of a Rotor/Seal System with the Dynamic Vibration Absorber. *Adv. Mech. Eng.* **2019**, *11*, 168781401881957. [[CrossRef](#)]
12. Qin, Y.; Zhao, Z.; Wang, Z.; Li, G. Study of Longitudinal-Vertical Dynamics for In-Wheel Motor-Driven Electric Vehicles. *Automot. Innov.* **2021**, *4*, 227–237. [[CrossRef](#)]
13. Qin, Y.; Wang, Z.; Yuan, K.; Zhang, Y. Comprehensive Analysis and Optimization of Dynamic Vibration-Absorbing Structures for Electric Vehicles Driven by In-Wheel Motors. *Automot. Innov.* **2019**, *2*, 254–262. [[CrossRef](#)]
14. Smith, M.C. Synthesis of Mechanical Networks: The Inerter. *IEEE Trans. Automat. Contr.* **2002**, *47*, 1648–1662. [[CrossRef](#)]
15. Wang, Q.; Zheng, Z.; Qiao, H.; De Domenico, D. Seismic Protection of Reinforced Concrete Continuous Girder Bridges with Inerter-Based Vibration Absorbers. *Soil Dyn. Earthq. Eng.* **2023**, *164*, 107526. [[CrossRef](#)]
16. Luo, J.; Macdonald, J.H.G.; Jiang, J.Z. Identification of Optimum Cable Vibration Absorbers Using Fixed-Sized-Inerter Layouts. *Mech. Mach. Theory* **2019**, *140*, 292–304. [[CrossRef](#)]
17. Sarkar, S.; Fitzgerald, B. Fluid Inerter for Optimal Vibration Control of Floating Offshore Wind Turbine Towers. *Eng. Struct.* **2022**, *266*, 114558. [[CrossRef](#)]
18. Hu, Y.; Wang, J.; Chen, M.Z.Q.; Li, Z.; Sun, Y. Load Mitigation for a Barge-Type Floating Offshore Wind Turbine via Inerter-Based Passive Structural Control. *Eng. Struct.* **2018**, *177*, 198–209. [[CrossRef](#)]
19. Li, Y.; Jiang, J.Z.; Neild, S. Inerter-Based Configurations for Main-Landing-Gear Shimmy Suppression. *J. Aircr.* **2017**, *54*, 684–693. [[CrossRef](#)]
20. Liu, X.; Jiang, J.Z.; Titurus, B.; Harrison, A. Model Identification Methodology for Fluid-Based Inerters. *Mech. Syst. Signal Process.* **2018**, *106*, 479–494. [[CrossRef](#)]
21. Liu, C.; Chen, L.; Lee, H.P.; Yang, Y.; Zhang, X. A Review of the Inerter and Inerter-Based Vibration Isolation: Theory, Devices, and Applications. *J. Frankl. Inst.* **2022**, *359*, 7677–7707. [[CrossRef](#)]
22. Shen, Y.; Chen, L.; Yang, X.; Shi, D.; Yang, J. Improved Design of Dynamic Vibration Absorber by Using the Inerter and Its Application in Vehicle Suspension. *J. Sound Vib.* **2016**, *361*, 148–158. [[CrossRef](#)]
23. Hu, Y.; Chen, M.Z.Q.; Sun, Y. Comfort-Oriented Vehicle Suspension Design with Skyhook Inerter Configuration. *J. Sound Vib.* **2017**, *405*, 34–47. [[CrossRef](#)]
24. Liu, X.; Jiang, J.Z.; Harrison, A.; Na, X. Truck Suspension Incorporating Inerters to Minimise Road Damage. *Proc. Inst. Mech. Eng. Part D J. Automob. Eng.* **2020**, *234*, 2693–2705. [[CrossRef](#)]
25. Liu, X.; Titurus, B.; Jiang, J.Z. Generalisable Model Development for Fluid-Inerter Integrated Damping Devices. *Mech. Mach. Theory* **2019**, *137*, 1–22. [[CrossRef](#)]
26. Firestone, F.A. A new analogy between mechanical and electrical systems. *J. Acoust. Soc. Am.* **1933**, *4*, 249–267. [[CrossRef](#)]
27. Wang, F.-C.; Chan, H.-A. Vehicle Suspensions with a Mechatronic Network Strut. *Veh. Syst. Dyn.* **2011**, *49*, 811–830. [[CrossRef](#)]
28. Shen, Y.; Shi, D.; Chen, L.; Liu, Y.; Yang, X. Modeling and Experimental Tests of Hydraulic Electric Inerter. *Sci. China Technol. Sci.* **2019**, *62*, 2161–2169. [[CrossRef](#)]
29. Shen, Y.; Han, J.; Zhang, Y.; He, T.; Yang, X.; Liu, Y.; Chen, L. The Invention Relates to an Electromagnetic Inertance Device. CN. Patent CN111089135B, 22 June 2021.
30. Kennedy, J.; Eberhart, R. Particle Swarm Optimization. In Proceedings of the ICNN'95—International Conference on Neural Networks, Perth, WA, Australia, 27 November–1 December 1995; Volume 4, pp. 1942–1948.

31. Eberhart, R.; Kennedy, J. A New Optimizer Using Particle Swarm Theory. In Proceedings of the MHS'95 Sixth International Symposium on Micro Machine and Human Science, Nagoya, Japan, 4–6 October 1995; pp. 39–43.
32. Shen, Y.; Jiang, J.Z.; Neild, S.A.; Chen, L. Vehicle Vibration Suppression Using an Inerter-Based Mechatronic Device. *Proc. Inst. Mech. Eng. Part D J. Automob. Eng.* **2020**, *234*, 2592–2601. [[CrossRef](#)]

Disclaimer/Publisher's Note: The statements, opinions and data contained in all publications are solely those of the individual author(s) and contributor(s) and not of MDPI and/or the editor(s). MDPI and/or the editor(s) disclaim responsibility for any injury to people or property resulting from any ideas, methods, instructions or products referred to in the content.